

Chapter 2

Self-assembly of InAs Quantum Dot Structures on Cleaved Facets

E. Uccelli, J. Bauer, M. Bichler, D. Schuh, J. J. Finley, G. Abstreiter,
and A. Fontcuberta i Morral

2.1 Introduction

Strain induced self-assembled quantum dots (QDs) have been extensively studied in the past decade. Their unique properties are mainly derived from the carrier confinement leading to atom-like energy level structure [1]. In this context, QDs are nanostructures that are indeed expected to have a great impact in optoelectronic devices. Methods to control the size and therefore the emission properties have been successfully developed, but the control of the position has shown to be a more difficult task. QDs usually nucleate randomly on a substrate by self-assembly [2], and methods to control the position are based on inducing a preferential nucleation of the self-organized dots at certain points on a surface. The different approaches range from the use of lithographically patterned substrates to vicinal surfaces [3, 4, 5, 6, 7, 8].

Alternatively, the Cleaved Edge Overgrowth technique has been used for the fabrication of atomically precise one and zero dimensional quantum structures. In this case, the quantum wires (QWRs) and dots are defined by the change in confinement potential at the intersection of one or two quantum wells (QWs), respectively [9, 10].

In this chapter, we present a different technique to deterministically control the position of self-assembled InAs QD arrays at the nanometer scale on (110) crystal surfaces. The method is a combination of self-assembly and the Cleaved Edge Overgrowth technique. In the first section, the growth technique is introduced. Then, in section 2.3 the results concerning the growth are shown. The optical properties of the self-assembled QDs are explained in Section 2.4. Finally, in Section 2.5, future prospects of the technique are presented.

2.2 Growth Technique

2.2.1 Cleaved Edge Overgrowth

The concept of Cleaved Edge Overgrowth (CEO) for the synthesis of quantum dot arrays (QDs) is illustrated in Fig. 2.1. The CEO technique was proposed by Störmer, Gossard and Wiegmann more than 20 years ago [10] and realized for the first time

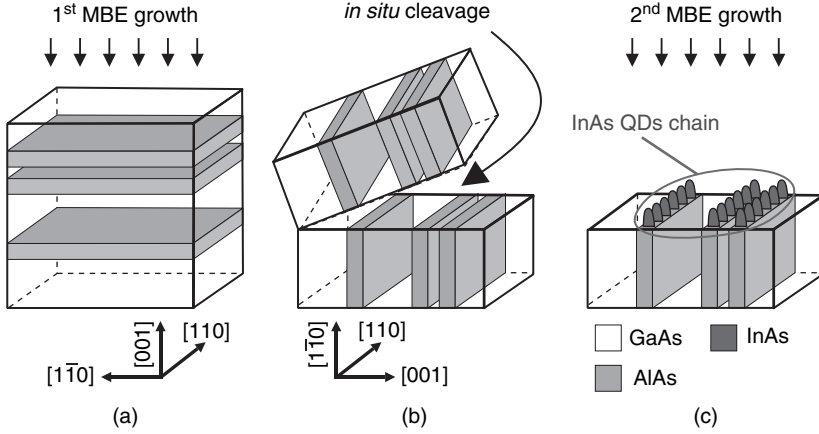


Fig. 2.1 The concept of the Cleaved Edge Overgrowth technique. (a) First MBE growth step, with the growth of AlAs/GaAs layers on a (100) wafer. (b) *in situ* cleave along the (110) plane. (c) Second MBE step with the overgrowth of InAs and formation of aligned InAs nanostructures on the cleaved facet

by Pfeiffer *et al.* at AT&T Bell Laboratories in 1990 [11]. It consists of two MBE growth steps separated by an *in situ* cleavage. The first MBE growth step is realized on a normal (001) substrate. Then, the sample is removed from the chamber and thinned to a thickness of 100–120 μm . The thin wafer is subsequently scribed and cleaved into rectangular pieces of 7 by 7 mm. A scratch along the $[1-10]$ direction is made where the future *in situ* cleave is to occur. After the cleavage along the $[110]$ direction inside the MBE chamber a new (110) surface is obtained, which is exposed to the second growth.

In our case, the first MBE step consists of the growth of an alternating series of AlAs and GaAs layers on a semi-insulating (001) GaAs oriented substrate (Fig. 2.1(a)). The substrate temperature is 650 $^{\circ}\text{C}$, the growth rate 1 $\text{\AA}/\text{s}$ for both GaAs and AlAs and the As_4 pressure 1.25×10^{-5} mbar. In the second MBE step, the material grown is InAs from 1 to 4 nominal monolayers (MLs). As it will be shown in this chapter, InAs tends to accumulate only on the AlAs regions, resulting in ordered arrays of InAs nanostructures such as quantum dots (QDs) and nanowires (NWs) (Fig. 2.1(c)). The successful growth of InAs on the cleaved facet has been found to have a particularly small process window: surface temperatures between 440 and 470 $^{\circ}\text{C}$, In rate lower than 0.15 $\text{\AA}/\text{s}$ and As_4 pressure between 4 and 6.5×10^{-5} mbar.

2.2.2 Mechanisms of QD Formation on (110) Surfaces

The substrate composition and orientation has an important effect on the morphology of epitaxially grown nanostructures. In a strained system such as InAs on GaAs, the surface energy of the underlying substrate strongly influences the way the energy

is released. Typically, the growth of InAs on (001) GaAs surfaces leads to the formation of QDs by the Stranski-Krastanov growth mechanism [2]. On the contrary, the same growth conditions on the (110) GaAs surfaces do not lead to QD formation. In this case, the strain is released by the formation of misfit dislocations, leading to much bigger islands [12, 13, 14]. An Atomic Force Microscopy measurement (AFM) of the surface morphology of InAs growth on (001) and (110) GaAs surfaces is shown in Fig. 2.2. Clearly, a high density of small, relatively uniform lens-shaped InAs islands are obtained on (100) substrates, while on (110) surfaces much larger trapezoidal islands are observed.

In order to investigate how the surface energy influences the way in which the stress is released in mismatch systems, growth of InAs has been investigated on the (110) facets of different materials. This is easily implemented by the CEO technique, as the composition of the (110) surface is given simply by the design of the (001) substrate. Indeed, one starts fabricating substrates composed of several layers of different materials, such as GaAs, $\text{In}_{0.3}\text{Ga}_{0.7}\text{As}$, $\text{Al}_{0.45}\text{Ga}_{0.55}\text{As}$ and AlAs. Subsequently, in the second MBE step, InAs growth is performed on the (110) facet of these materials and the surface morphology is investigated by AFM.

The structure of the substrate is as follows: two different layer sequences (superlattices¹, in the following denoted as SL) of $\text{In}_{0.3}\text{Ga}_{0.7}\text{As}$ -GaAs and AlAs-GaAs layers were grown on a semi-insulating GaAs (001) substrate. They are separated by a GaAs layer. (Sample-A). Here, SL1 consists of 5 periods of 20 nm $\text{In}_{0.3}\text{Ga}_{0.7}\text{As}$ and 40 nm GaAs, whilst SL2 is composed by 10 periods 20 nm AlAs and 20 nm GaAs. After *in situ* cleaving of the substrate in the MBE chamber, different amounts

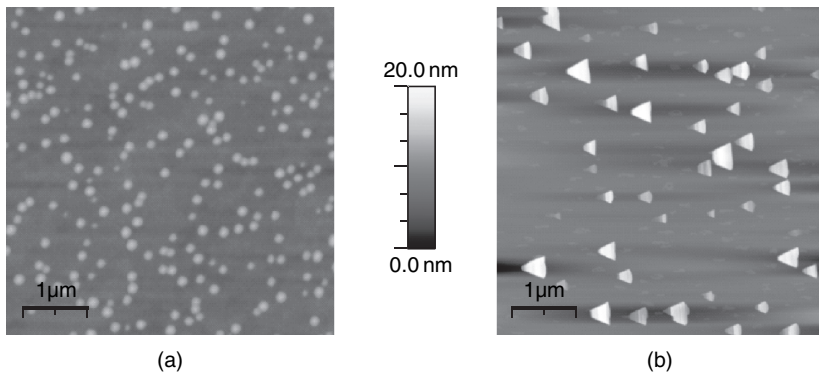


Fig. 2.2 Surface topology of InAs grown on (001) and (110) GaAs surfaces by AFM. (a) On (001) GaAs: high density formation of lens shaped QDs (b) Larger triangular and trapezoidal islands formation on (110) oriented GaAs surface

¹ For simplicity these layer sequences are called “superlattices” (SL) within this work. It has to be emphasized that this does not refer to the concept of overlapping wavefunctions and miniband formation but that this expression is only used to highlight the periodicity of the alternating layers grown.

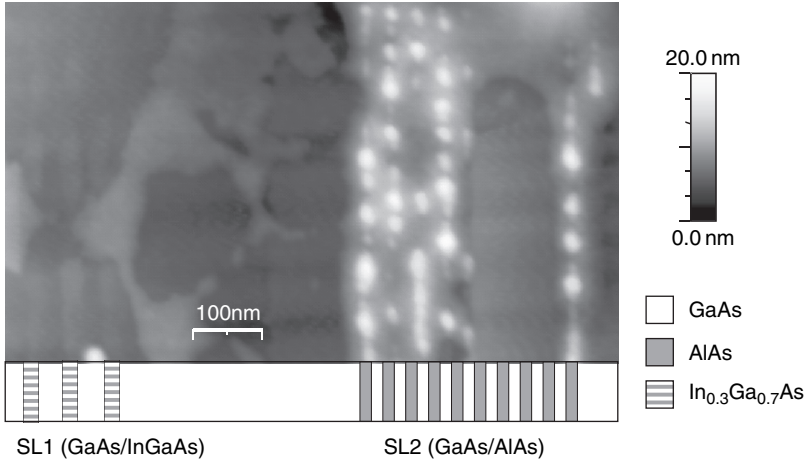


Fig. 2.3 Effect of the surface composition on the nucleation of QDs: Atomic Force Microscope measurement of the (1–10) surface of Sample A with both In_{0.3}Ga_{0.7}As/GaAs and AlAs/GaAs heterostructure for QDs template. Only on top of the AlAs stripes three dimensional QD like structures have been formed, after deposition of a nominal thickness of 3 ML InAs at a surface temperature of 460 °C

of InAs (namely 2–3–4 ML) were deposited directly on the exposed (1–10) surface at different growth temperatures (450–470 °C).

Figure 2.3 is a typical AFM measurement of the surface after deposition of 3 ML of InAs. As depicted, three dimensional islands or quantum dots (QDs) form on some of the stripes. QD formation is only observed on the AlAs stripes, and no QD nucleation has been observed on the In_{0.3}Ga_{0.7}As stripes. The lack of QD nucleation onto In_{0.3}Ga_{0.7}As–GaAs SLs was a surprising observation, as it seems to contradict some published theoretical predictions and experimental works [15, 16]. However, it cannot be excluded that the MBE growth conditions were simply inappropriate ones for nucleation of QDs on (110) In_{0.3}Ga_{0.7}As. The same growth was tried on AlAs/Al_{0.45}Ga_{0.55}As superlattices. As in the case of AlAs/GaAs, only on the AlAs stripes QDs were observed.

In the remainder of the chapter, we will focus on the growth of InAs nanostructures on the AlAs–GaAs (110) system.

2.3 Experimental Results

2.3.1 General Characteristics

To investigate the growth characteristics of InAs on AlAs stripes, a second substrate was used, composed of 5 different AlAs–GaAs SLs separated by a 1 μm GaAs layer (Sample-B). Each SL consists of 10 layers of AlAs separated by a 70 nm thick GaAs stripe. The thickness of the AlAs layers varied from 20 nm (SL1) up to 40 nm (SL5).

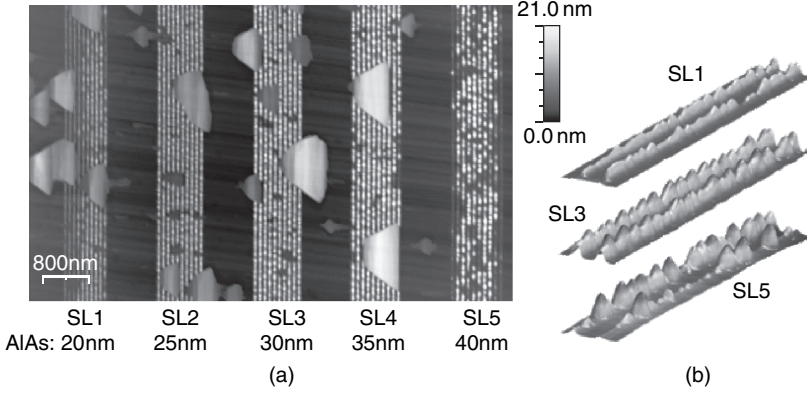


Fig. 2.4 General morphology of InAs growth on AlAs/GaAs SLs: (a) Atomic Force Microscopy of InAs QDs grown on a cleaved facet with AlAs/GaAs superlattices with 5 different AlAs stripe thicknesses (indicated on the picture). (b) 3-dimensional representation of the QDs grown on the stripes for three different stripe thicknesses

A typical Atomic Force Microscopy measurement of the cleaved-edge surface after the nominal growth of 3.2ML of InAs is presented in Fig. 2.4(a). QDs have formed on the AlAs stripes for all SLs. For a more clear representation, a three-dimensional image of some of these arrays is presented in Fig. 2.4(b). Also visible in Fig. 2.4(a) are much larger triangular islands with height of some monolayers. These nanostructures correspond to the islands that have been already observed in MBE grown structures on (110) GaAs substrates [17].

In order to get a quantitative characterization of the morphology of the QDs, a detailed statistical analysis of the dot dimensions has been performed. As can be seen from Fig. 2.5(a), the lateral size of the QDs follows the thickness of the underlying AlAs stripe. The smallest dots are nucleated on SL1 (AlAs 20 nm) and largest dots on SL5 (AlAs 40 nm). As it will be shown in next section and according

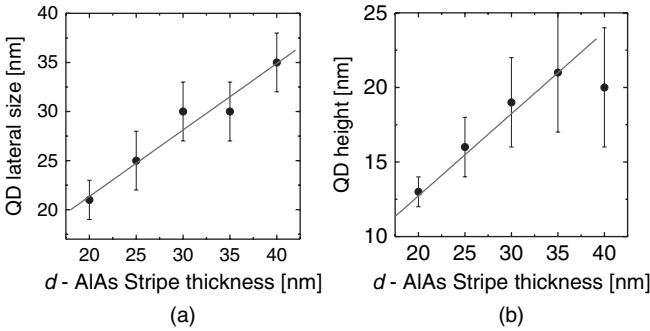


Fig. 2.5 Dimensions of the QDs as a function of the AlAs stripe thickness: (a) Lateral size (b) Height

to Fig. 2.5(b), the height of the dots increases linearly with the AlAs stripe thickness (from 13 nm on SL1 up to more than 20 nm for dots on SL4 and SL5). The average linear dot density along the AlAs stripes has also been estimated, but no specific dependency for density versus AlAs thickness has been found. For the calculations, regions with trapezoidal defects have been excluded, as these are considered to be strong perturbations to the dominant growth mode.

2.3.2 Growth Studies of the QD Formation Mechanism

In order to gain insight into the growth mechanisms of preferential migration of InAs on (110) AlAs regions and nucleation of QDs, a series of systematic growth runs were performed. The density and morphology of InAs nanostructures was studied as a function of the AlAs stripe width and nominal InAs thickness. For this particular study, the substrate (labeled as Sample-C) consisted of a series of AlAs stripes of thicknesses varying from 3 nm to 42 nm, separated by 70 nm GaAs spacers. A typical AFM measurement of a sample grown on this kind of superlattice is illustrated in Fig. 2.6. From the intensity scale, it is clear that the QD height increases with the AlAs stripe thickness. Indeed, on the thinner stripes the height does not differ much from the neighboring GaAs, which means that there seems to be almost no accumulation of InAs in these regions and no QDs are formed. In contrast, for the largest stripes the QDs reach heights up to 22 nm.

The size uniformity of QDs within a stripe was studied by measuring the height distribution from the AFM measurements. A variance of less than 17% was found in all cases. A much narrower size distribution would be highly desirable.

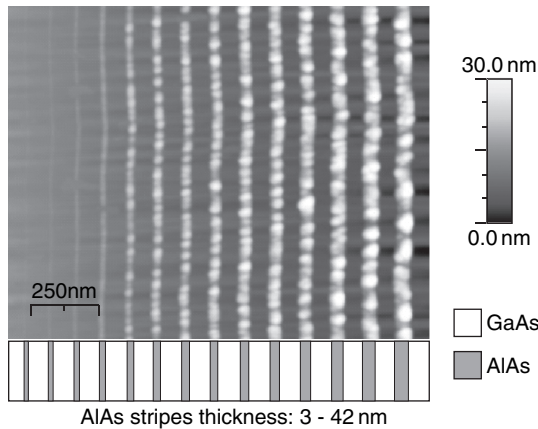


Fig. 2.6 Nucleation of InAs on AlAs stripes with increasing thickness: (a) AFM picture of Sample-C overgrown by 2.0 ML InAs. Formation of nanowires on narrow AlAs stripes as well as QDs chain on AlAs stripe equal and larger than 15 nm

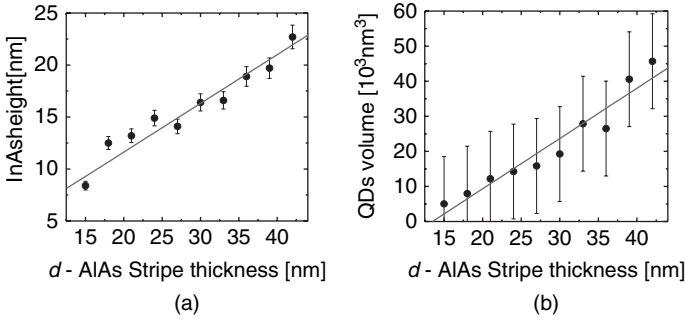


Fig. 2.7 Morphology of the InAs QDs for increasing AlAs stripe thickness relation to Fig. 2.6: (a) height and (b) volume of the QD's. The QD nucleation onset (Volume close to zero) occurs at $d = 15 \text{ nm}$

The mean height and volume of the QDs is plotted in Fig. 2.7 as a function of the stripe thickness, d . The QD volume and height increase linearly with the AlAs stripe thickness. This means that the nominal thickness is distributed unevenly through the surface. InAs tends to accumulate on AlAs stripes, increasing the total InAs effective thickness. This effect is linearly dependent on d . As it will be shown in the section 2.3.3, this is a consequence of the much lower diffusion coefficient and lifetime of the In-adatoms on (110) AlAs with respect to (110) GaAs. As the effective InAs thickness depends on d , the critical thickness needed for the nucleation of QDs, t_c , is achieved only on some of the stripes. On the thinnest stripes, the effective thickness lies below t_c and no QDs can form. This is exactly what it is observed experimentally. As shown in Figs. 2.6 and 2.7, in good agreement with this expectation, an onset of nucleation for the QDs is observed at a stripe thickness of 15 nm.

Even if the QDs lateral size and height scales with the AlAs stripe thickness, it is common sense that this can only occur up to certain values. Indeed, after a certain AlAs thickness, a transition to 2D growth should occur. In order to understand where this limit value lies, a second substrate (Sample-D) was designed with 80 and 100 nm wide AlAs stripes. An AFM measurement after growth of 3.2 ML is shown in Fig. 2.8. In this case, the single QD array is not observed anymore. However, instead of observing a transition to a random 2D arrangement, the QDs continue to grow aligned along the stripes. The difference here is that the QDs tend to nucleate next to the interface between stripes. This result may indicate that the QD formation does not follow exactly a Stranski-Krastanov growth mechanism [2] and deserves to be studied in more detail in the future.

2.3.3 Discussion of the Growth Mechanism

In this section we demonstrate, with a simple model, that the selectivity of the InAs nucleation on (1-10) surfaces can be understood as a consequence of the different

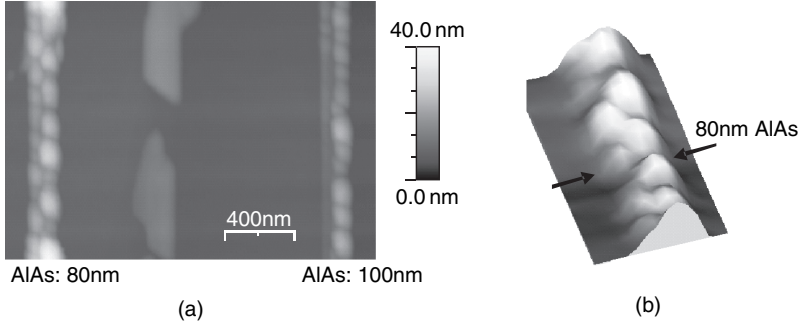


Fig. 2.8 Formation of QD pairs on thicker AlAs stripes: (a) AFM picture of Sample-D overgrown by nominally 3.2 ML of InAs. On very broad AlAs stripe (>80 nm) InAs can nucleate in bi-QD chain. (b) 3D picture of bi-QD chain

desorption rate and mobility of the impinging In-adatoms on AlAs and GaAs (110) growth surfaces [18]. As it has been previously reported, the diffusion length of the In-adatoms is more than three times larger on (001) Ga-rich surfaces than on Al-rich (001) surfaces (35 nm vs. 10 nm) [19]. This ratio remains almost constant on (Ga,Al)As (110) surfaces, but the absolute diffusion length increases in each case by more than a factor of 30 [15, 20] ($>1 \mu\text{m}$ vs. 350 nm). As a consequence, it is expected that In-adatoms would naturally tend to accumulate on the AlAs stripes rather than on the GaAs regions.

A very simple model can help understand how this happens. The main processes occurring at the growing surface are depicted in Fig. 2.9(a). First, Arsenic is a highly volatile atom which is continuously adsorbed and desorbed on the surface. On the contrary, after impinging on the surface, Indium diffuses along the surface before being incorporated in a film or desorbed. Depending on the temperature, surface composition and/or crystal orientation, the diffusion length of In can vary from several nm to microns. It has been shown that the In-adatoms mobility and desorption rate on Al-containing layers is lower [19, 20]. As it will be shown in the following, the difference in mobility and desorption rate leads to a higher effective mass flow towards the AlAs stripes [21]. We start by considering movement of In-adatoms in one dimension. Resulting from the combination of random walk and interaction with

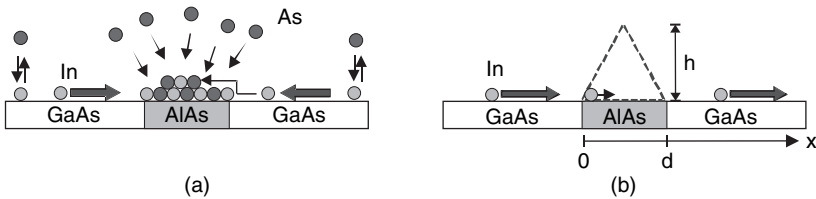


Fig. 2.9 Schematics of dynamics of In and As-adatoms on the growing surface (a) Mechanism for the preferential nucleation of InAs QDs on top of AlAs (110) stripes; (b) Schematics of the diffusion model presented

the underlying substrate, the effective movement of In-adatoms can be described by the diffusion equation with an effective diffusion coefficient, D . The diffusion coefficient depends on the type of material underneath and is significantly smaller for AlAs than for GaAs [19].

As described above, we assume that the movement of In-adatoms follows the equation

$$x(t) = x_o + \sqrt{D \cdot t} \quad (2.1)$$

where D is the diffusion coefficient that varies on top of AlAs and GaAs surface, and t is time. Per unit time, the probability of an In atom precipitating to form InAs is inversely proportional to the lifetime (τ) of In-adatom on the material. This means that for a certain time Δt , the amount of deposited In atoms will be proportional to this probability. If one now approximates the geometry of the QDs as triangular, the amount of InAs on top of the AlA region, V_{InAs} , will be:

$$V_{InAs} = \frac{\Delta t}{\tau_{AlAs}} = \frac{1}{2}h \cdot d \quad (2.2)$$

where h and d are the height and width of the QDs.

Now, let us consider a single In ad-atom arriving at the interface between GaAs and AlAs ($x = 0$) and moving towards $x > 0$. By using the diffusion equation for the movement of In-adatoms (Eq. 2.1), one can calculate the average time Δt that an In ad-atom would spend on the AlAs stripe. By introducing this value into Eq. 2.2 it is then possible to calculate the average height of the QDs as a function of the AlAs stripe thickness d :

$$h(d) \sim \frac{d}{D_{AlAs} \tau_{AlAs}} \quad (2.3)$$

The diffusion of In-adatoms on GaAs is not considered in this simple calculation, which is based on the assumption that the diffusion coefficient and lifetime of In-adatoms in (110) GaAs are much larger than in AlAs ($D_{GaAs} \gg D_{AlAs}$ and $\tau_{GaAs} \gg \tau_{AlAs}$). However, such simple calculations can help to understand intuitively why the effective thickness of InAs increases linearly with d and in what sense the values of D and τ play a role in the process.

2.4 Optical Properties

In this section, the optical properties of the InAs QDs on the AlAs stripes are investigated by micro-photoluminescence spectroscopy (μ PL). In section 2.4.1, preliminary measurements comparing the substrate response with and without the InAs QDs will be presented. Then, in section 2.4.2 the properties of ensembles of QDs as

a function of size will be presented. In section 2.4.3, the dependence of PL with the excitation will be shown for an ensemble of a few ODs. Finally, in section 2.4.4 the temperature dependence of the PL will be briefly discussed.

The samples were mounted in a vertical holder inside a liquid helium cryostat. PL was excited with a HeNe laser (632 nm), incident perpendicularly to the (1–10) surface. Due to the confocal excitation and collection geometry, the spatial resolution in both excitation and detection channels was 1.5 to 2.5 μm . The measurements were performed at temperatures from 10 to 85 K. Two different substrates (Sample-E and Sample-F) were investigated. Their structure is depicted schematically in Fig. 2.10(a–b). Sample-E consists of four spatially separated AlAs/GaAs SLs (SL1: five periods of 32 nm AlAs and 68 nm GaAs; SL2: five periods of 20 nm AlAs and 40 nm GaAs; SL3: five periods of 11 nm AlAs and 22 nm GaAs; SL4: ten periods of 20 nm AlAs and 20 nm GaAs) grown on semi-insulating (001) GaAs. Sample-F consists of a stack of SLs with different AlAs thicknesses. Each SL consists of a stack of 10 AlAs/GaAs, the thickness of AlAs varies from 20 to 40 nm, while the thickness of GaAs was kept at 70 nm.

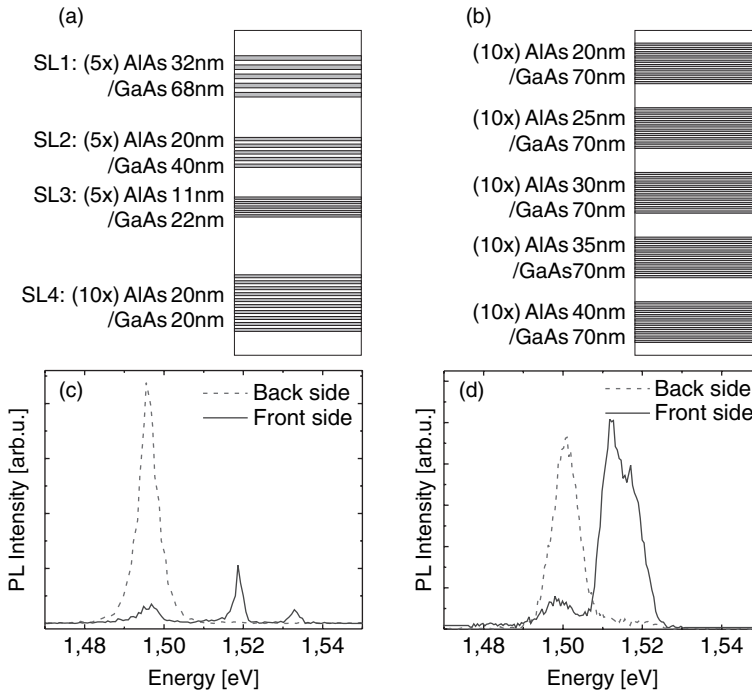


Fig. 2.10 Photoluminescence of the substrates: (a)–(b) Schematics of the substrate geometry of Sample-E and F. (c)–(d) PL-spectra from both front side (solid line) and back side (dashed line) of the substrates

2.4.1 Optical Response of the Substrates

Before studying in detail the optical properties of the InAs nanostructures, the macro-photoluminescence response of the underlying substrate was recorded, in order to have an optical reference to clearly distinguish the GaAs bulk material and the MBE grown layer sequences from the μ -PL measurements of the overgrown material.

Photoluminescence measurements of Sample-E and Sample-F are shown in Fig. 2.10(c–d). In all substrates, the epi-side was not thicker than 10 μm , much thinner than the thickness of the wafer (100–150 μm). Since the laser exciting perpendicular to the (001) surface of the substrate has a finite penetration depth [22], only material near the surface can contribute to the PL signal. Therefore, measurements on both front- and back-side of the samples can correspond respectively to the MBE grown layer sequences and the GaAs bulk material, giving a spectral fingerprint of the epitaxially grown layer.

The spectra confirm that the luminescence characteristics are strongly different. Front-side spectra show generally a stronger emission (single peak or a couple of peaks) around 1.515 eV and an emission with low intensity close to 1.50 eV. Back-side spectra show only one emission line near 1.50 eV. The peak at 1.519 eV (Fig. 2.10(c)) corresponds to GaAs energy gap [23], while we suggest that the peak at 1.533 eV (above the gallium arsenide band gap) arises from the weak quantum confinement effect in 20 nm GaAs stripe. This peak has been observed only in the Sample-E. According to [23], peaks at 1.517 eV and at 1.512 eV (Fig. 2.10(d)) arise from free and bound exciton (in GaAs). The peak around 1.499 eV (front and back side in both figures) is caused by the presence of carbon impurities in GaAs [23]. In Sample-F, the exciton peak of GaAs is significantly broadened and seems to be composed of more than one peak, shifting the whole band to lower energies. We attribute this shift to the presence of tensile stress of the GaAs sandwiched between the multiple layers of AlAs (difference in the lattice constant). To illustrate this phenomenon we have added the μPL scan of the (1–10) side of the substrate for Sample-F. It is clear from Fig. 2.11 that the shift increases in the growth direction with the number of SLs.

2.4.2 Optical Properties of Ensemble of QDs

The optical properties of QDs resulting from the growth of 3 ML of InAs capped by 50 nm of GaAs on both Sample-E and Sample-F were investigated by μ -PL spectroscopy. As has been presented in section 2.3, the size of the QDs is predetermined by the thickness of the AlAs stripe, which should be reflected directly in the optical properties. Additionally, the measurements should also give some measurement of the size homogeneity.

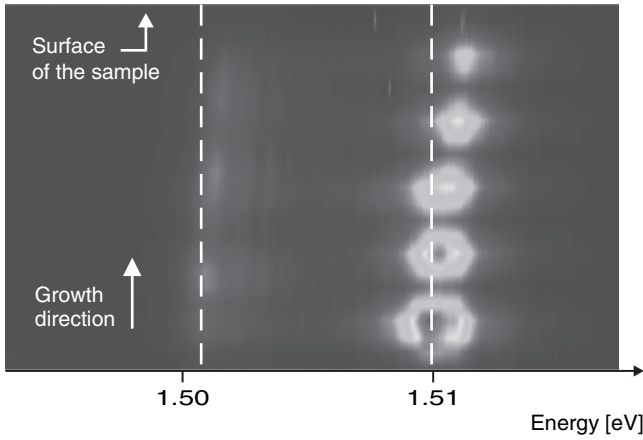


Fig. 2.11 μ -PL scan of substrate F: The excitonic peak clearly shifts to higher energies as more SLs are added

A $2.5\,\mu\text{m}$ excitation spot was scanned across the (1–10) surface along the [001] direction of Sample-E in order to collect the PL response of the QDs arising from the different SLs. A strong luminescence signal coming from the excitonic recombination in InAs QDs was observed around 1.3 eV. The spectra in Fig. 12 correspond to the PL signal excited with a power of $\sim 70\text{ mW/cm}^2$. In the figure, two photoluminescence spectra are presented. They were collected with the laser spot positioned on two different SLs. The peak mainly centered at 1.328 eV (labeled PL1) corresponds to the measurement realized on the QDs grown on 32 nm AlAs stripes (SL1). The second spectrum corresponds to the PL signal from the QDs grown on the 20 nm AlAs stripes (SL4) and consists of a main peak centered at 1.365 eV (labeled PL4). As expected, smaller QDs emit at slightly higher energies. In both spectra a second peak is present; whose origin is the PL emission of the QDs in the neighboring SLs. Both spectra are characterized by small line width

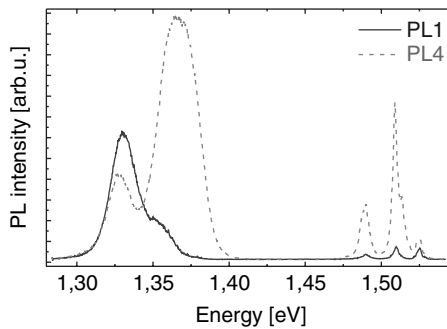


Fig. 2.12 μ -PL measurements of ensemble of QDs grown on Sample-E: spectra taken on different SLs, with AlAs stripe thickness of 32 nm (solid line) and 20 nm (dashed line). Both peaks present a clear Gaussian shape at 1.324 (1.3625) eV and show very narrow FWHM of 17.7 (25.0) meV

(~ 25 meV and ~ 18 meV), meaning a relatively good size homogeneity of the dots, in agreement with the AFM analysis presented above [24]. It is interesting to note that the obtained values for the line width are very close to some other very narrow measured values in InAs self-assembled QDs ensembles by other groups (~ 16 meV e.g.[25,26]).

2.4.3 Power Dependence Measurements of Single QDs

In order to verify the QD nature of the InAs islands, we performed PL spectroscopy of single dots. For that, we scanned the stripes of low QD density with a $1.5\ \mu\text{m}$ laser spot. In certain areas of low dot density, we found sharp line luminescence indicating PL of few individual dots. In these areas we performed power dependent μ -PL measurements. The power was varied from 1.8 to $1800\ \mu\text{W}/\text{cm}^2$. In Fig. 2.13, we show the result of such a measurement, where one quantum dot is contributing to the spectra. Only a single emission line at $1.308\ \text{eV}$ is observed at low excitation power. The linear power dependence of the intensity identifies it as arising from a single exciton (X^0). In addition, this line is an emission doublet, possibly due to elongation of the quantum dots along the AlAs layer and the resulting anisotropic electron-hole exchange interaction [27]. Upon increasing the excitation power density, several sharp lines at lower ($1.3044\ \text{eV}$) and higher ($1.3135\ \text{eV}$, $1.3148\ \text{eV}$, $1.3166\ \text{eV}$ and $1.3182\ \text{eV}$) energies emerge. The intensity of the emission line at $1.3044\ \text{eV}$ increases roughly quadratically with excitation power density and dominates the spectra for the highest excitation densities investigated. This characteristic behavior identifies the peak as arising from bi-exciton ($2X$) recombination in the dot [28]). The other lines observed at high power arise from multi exciton complexes (mX) and possibly also charged excitons [29]. In conclusion, we have observed single dot like luminescence that confirms the QD nature of the InAs islands.

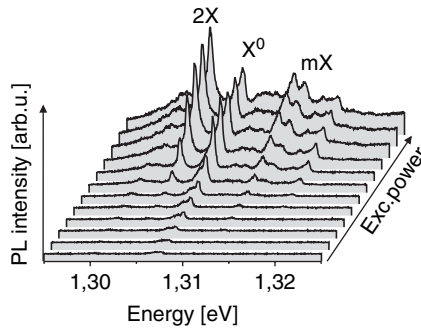


Fig. 2.13 PL spectra taken at different excitation power with spot laser localized only on few QDs

2.4.4 Temperature Dependence Measurements

A temperature series of the PL was realized on Sample-F to further elucidate the optical properties. The sample temperature was controlled by a resistive heater together with a silicon temperature diode placed near the sample in the cryostat. Care was taken to ensure that the temperature of the sample was stable. For all measurements, the excitation power ($\sim 4 \mu\text{W}/\text{cm}^2$) and the scanning position were kept constant. Figure 2.14 shows spectra recorded on the SL with AlAs stripes of 35 nm thickness of Sample-F.

The measurements clearly reveal a decreasing PL intensity as well as an increasing broadening of the PL, with rising temperature. This behavior can be explained as the enhancement of carrier escape processes from the quantum dot energy levels to the continuum states of the surrounding material at higher temperatures [1]. Due to the three-dimensional confinement, the localization energy for electron and hole is higher for QDs than for QWRs or QWs. Indeed, the integrated intensity of the PL lines I should follow the Arrhenius relation [30]:

$$I(T) = I_o \cdot \exp\left(\frac{-E_{loc}}{K_B T}\right) \quad (2.4)$$

where E_{loc} is the confinement energy, K_B the Boltzman constant and T the temperature. As a consequence, the escape rate for thermally activated carriers is smaller and hence the increase in PL line broadening is also smaller for QDs than for QWs or QWRs. This general behavior can be observed in Fig. 2.14. From the measurements, an E_{loc} of 18 meV was obtained. This seems to be a very low value (as 100 meV was expected, e.g. [31]). One possible origin could be the intermixing of the InAs dots with the surrounding materials, but more detailed investigations will be realized in the future in order to a better understanding.

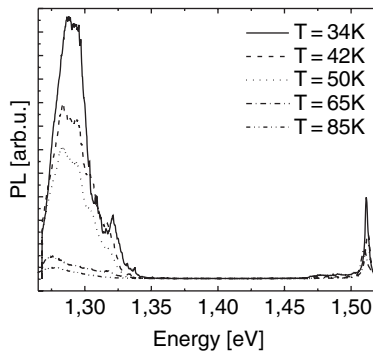


Fig. 2.14 Temperature dependent spectra taken from ensemble of QDs on Sample-F

2.5 Perspectives and Future Work

The successful control of the synthesis of QD arrays opens many perspectives in the fields of physics, electronics and information technology. It is relatively straightforward to imagine different devices that are enabled by this technique. Some of them will be briefly presented in this section.

One possibility is the use of the arrays as the channel of a transistor to investigate the transport properties of a QD chain. This can be achieved if the AlAs quantum well on which the QDs are nucleated contains a two dimensional electron gas (2DEG) and by depositing a thin gate on the (001) surface. As shown in Fig. 2.15, it is possible to separate the 2DEG into two electron reservoirs by applying a gate voltage, the distance between being defined by the gate thickness. Theoretically, the electronic transport from side to side of the 2DEG is only possible through the QD array.

Other possibilities are to use the optical functionality of the QDs for quantum information processing. Indeed, one can exploit the optical excitations in QDs to obtain coherent manipulation of two excitonic levels within one dot but also between coupled dots. The extrapolation to several dots is enabled by the work presented in this chapter and opens up a large variety of experiments where the coupling between single dots and chains can be investigated.

Finally, the structural characteristics of the QD arrays will need more careful investigation. In that respect, cross-sectional High Resolution Transmission Electron Microscopy and Raman spectroscopy measurements will be realized. These studies will provide not only information on the crystalline structure of the QDs, but also insights on the formation mechanism of the QDs. With these studies, we expect to answer the question of whether the QDs nucleation occurs via a Stranski-Krastanov or by an AlAs intermixing process.

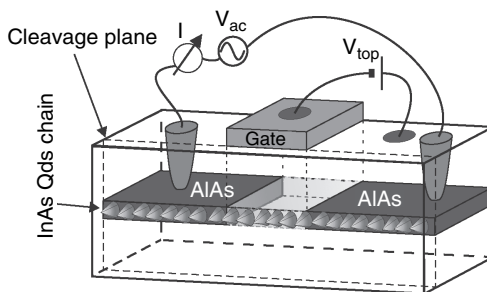


Fig. 2.15 Schematics of the configuration for a QD chain transistor device

Acknowledgments This work was financially supported by the Deutsche Forschungsgemeinschaft (DFG) in the framework of SFB 631 TP B1, by the Bundesministerium für Bildung, Wissenschaft, Forschung und Technologie (BmBF) through the Grant NanoQUIT-01BM469 and by the EC-Research Training Network COLLECT, HPRN-CT-2002-00291. The Marie Curie Excellence Grant program is also acknowledged (Project MEXT-CT-2006-042721, “SENFED”).

References

1. Bimberg D, Grundmann M, Ledentsov NN (1999) Quantum Dot Heterostructures. John Wiley and Sons, Chichester
2. Stranski IN, Krastanow L (1938) Zur Theorie der orientierten Abscheidung von Ionenkristallen aufeinander. Sitzungsberichte der Akademie der Wissenschaften in Wien, Mathematisch-Naturwissenschaftliche Klasse, Abt. IIB, 146(1–10):797
3. Nötzel R, Ploog KH (2001) MBE of quantum wires and quantum dots. *J. Cryst. Growth* 227–228:8–12
4. Kim HJ, Park YJ, Park YM, Kim EK, Kim TW (2001) Fabrication of wirelike InAs quantum dots on 2°-off GaAs (100) substrates by changing the thickness of the InAs layer. *Appl. Phys. Lett.* 78:3253–3255
5. Leon R, Chaparro S, Johnson SR, Navarro C, Jin X, Zhang YH, Siegart J, Marcinkevicius S, Liao XZ, Zou J (2002) Dislocation-induced spatial ordering of InAs quantum dots: Effects on optical properties. *J. Appl. Phys.* 91:5826–5830
6. Bhat R, Kapon E, Hwang DM, Koza MA, Yun CP (1988) Patterned quantum well heterostructures grown by OMCVD on non-planar substrates: Applications to extremely narrow SQW lasers. *J. Cryst. Growth* 93:850–856
7. Gerardot BD, Subramanian G, Minvielle S, Lee H, Johnson JA, Schoenfeld WV, Pine D, Speck JS, Petroff PM (2002) Self-assembling quantum dot lattices through nucleation site engineering. *J. Cryst. Growth* 236:647–654
8. Songmuang R, Kiravittaya S, Schmidt OG (2003) Formation of lateral quantum dot molecules around self-assembled nanoholes. *Appl. Phys. Lett.* 82:2892–2894
9. Schedelbeck G, Wegscheider W, Bichler M, Abstreiter G (1997) Coupled quantum dots fabricated by cleaved edge overgrowth: From artificial atoms to molecules. *Science* 278:1792–1795
10. Wegscheider W (2005) Cleaved Edge Overgrowth, T-Shaped Quantum Wires and Dots. In: Bryant GW, Solomon GS (eds) *Optics of Quantum Dots and Wires*. Artech House, Boston, pp 271–314
11. Pfeiffer L, West KW, Stormer HL, Eisenstein JP, Baldwin KW, Gershoni D, Spector J (1990) Formation of high quality two-dimensional electron gas on cleaved GaAs. *Appl. Phys. Lett.* 56:1697–1699
12. Belk JG, Sudijono JL, Zhang XM, Neave JH, Jones TS, Joyce BA (1997) Surface contrast in two dimensionally nucleated misfit dislocations in InAs/GaAs(110) heteroepitaxy. *Phys. Rev. Lett.* 78:475–478
13. Belk JG, Pashley DW, McConville CF, Joyce BA, Jones TS (1998) Surface morphology during strain relaxation in the growth of InAs on GaAs(110). *Surf. Sc.* 410:82–98
14. Joyce BA, Jones TS, Belk JG (1998) Reflection high-energy electron diffraction/scanning tunneling microscopy study of InAs growth on the three low index orientations of GaAs: Twodimensional versus three-dimensional growth and strain relaxation. *J. Vac. Sci. Technol. B*, 16:2373–2380
15. Wasserman D, Lyon SA (2004) Cleaved-edge overgrowth of aligned quantum dots on strained layers of InGaAs. *Appl. Phys. Lett.* 85:5352–5354
16. Zhao C, Chen YH, Cui CX, Xu B, Sun J, Lei W, Lu LK, Wang ZG (2005) Quantum-dot growth simulation on periodic stress of substrate. *J. Chem. Phys.* 123:094708–094711

17. Yoshita M, Oh JW, Akiyama H, Pfeiffer LN, West KW (2003) Control of MBE surface step-edge kinetics to make an atomically smooth quantum well. *J. Cryst. Gr.* 251:62–67
18. Shchukin VA, Ledentsov NN, Bimberg D (2004) *Epitaxy of nanostructures*, Springer-Verlag, Berlin
19. Ballet P, Smathers JB, Yang H, Workman CL, Salamo GJ (2001) Control of size and density of InAs/(Al,Ga)As self-organized islands. *J. Appl. Phys.* 90:481–487
20. Lobo C, Leon R (1998) InGaAs island shapes and adatom migration behavior on (100), (110), (111), and (311) GaAs surfaces. *J. Appl. Phys.* 83, 4168–4172
21. Bauer J, Schuh D, Uccelli E, Schulz R, Kress A, Hofbauer F, Finley JJ, Abstreiter G (2004) Long-range ordered self-assembled InAs quantum dots epitaxially grown on (110) GaAs. *Appl. Phys. Lett.* 85:4750–4752
22. Gustafsson A, Pistol ME, Montelius L, Samuelson L (1998) Local probe techniques for luminescence studies of low-dimensional semiconductor structures. *J. Appl. Phys.* 84:1715–1775
23. Pavesi L, Guzzi M (1994) Photoluminescence of $\text{Al}_x\text{Ga}_{1-x}\text{As}$ alloys. *J. Appl. Phys.* 75:4779–4842
24. Schuh D, Bauer J, Uccelli E, Schulz R, Kress A, Hofbauer F, Finley JJ, Abstreiter G (2005) Controlled positioning of self-assembled InAs quantum dots on (110) GaAs. *Physica E* 26:72–75
25. Costantini G, Manzano C, Songmuang R, Schmidt OG, Kern K (2003) InAs/GaAs (001) quantum dots close to thermodynamic equilibrium. *Appl. Phys. Lett.* 82:3194–3196
26. Yang T, Tatebayashi J, Tsukamoto S, Nishioka M, Arakawa Y (2004) Narrow photoluminescence linewidth (<17 meV) from highly uniform self-assembled InAs/GaAs quantum dots grown by low-pressure metalorganic chemical vapor deposition. *Appl. Phys. Lett.* 84:2817–2819
27. Bayer M, Ortner G, Stern O, Kuther A, Gorbunov AA, Forchel A, Hawrylak P, Fafard S, Hinzer K, Reinecke TL, Walck SN, Reithmaier JP, Klopff F, Schäfer F (2002) Fine structure of neutral and charged excitons in self-assembled In(Ga)As/(Al)GaAs quantum dots. *Phys. Rev. B* 65:195315–195337
28. Brunner K, Abstreiter G, Böhm G, Tränkle G, Weimann G (1994) Sharp-Line Photoluminescence and Two-Photon Absorption of Zero-Dimensional Biexcitons in a GaAs/AlGaAs Structure. *Phys. Rev. Lett.* 73:1138–1141
29. Findeis F, Zrenner A, Böhm G, Abstreiter G (2000) Optical spectroscopy on a single InGaAs/GaAs quantum dot in the few-exciton limit. *Solid State Comm.* 114:227–230
30. Kapteyn CMA, Lion M, Heitz R, Bimberg D, Brunkov PN, Volovik BV, Konnikov SG, Kovsh AR, Ustinov VM (2000) Room-temperature 1.3 mm emission from InAs quantum dots grown by metal organic chemical vapor deposition. *Appl. Phys. Lett.* 76:1573–1575
31. Chu L, Zrenner A, Bichler M, Böhm G, Abstreiter G (2001) Intersubband photocurrent spectroscopy on self-assembled In(Ga)As/GaAs quantum dots. *Phys. Stat. Sol. (b)* 224: 591–594

Self-Assembled Quantum Dots

Wang, Z.M. (Ed.)

2008, XII, 468 p. 250 illus., Hardcover

ISBN: 978-0-387-74190-1